RESEARCH REPORT

VTT-R-00737-11

Smart Control of Wind Power Plant

Authors: Tuomas Haarnoja

Confidentiality: Public

Report's title Smart Control of Wind Power Plant	
Customer, contact person, address VTT	Order reference
Project name Wind power plants – knowledge increase of noise and control issues	Project number/Short name 73794 / WPPNoCo
Author(s) Tuomas Haarnoja	Pages 27
Keywords wind power plant, control, individual pitch control, smart blade	Report identification code VTT-R-00737-11

Summary

One of the biggest causes of mechanical failures in wind turbines is the periodical disturbing moments that load the blades, the drivetrain, and the tower. The main cause for these loads is wind shear: the stronger wind at the higher altitude exerts a flapwise force to the blades pointing upwards and weaker force to the others. Consequently, the net force of the rotor is not aligned with the drivetrain resulting in a tilt and yaw moments that varies periodically with the rotor azimuth angle. These loads not only increase the need for maintenance but also forces designers to use stronger and thus more expensive and heavier materials, which, in turn, has a direct impact to the cost of energy.

There exist essentially two approaches for reducing the moments caused by wind shear: smart blades and Individual Pitch Control (IPC). Both of the methods are based on the idea of controlling the aerodynamic force of each blade individually in order to keep the flapwise force constant during a revolution. Smart blade consists of sensors and actuators that can be used to modify the airfoil characteristics dynamically. The solutions vary from flaps to more complex structures. Most of the actuators have wide bandwidth compared to the disturbance frequencies in modern wind turbines. On the other hand, IPC has a narrower bandwidth but it does not require any changes to existing rotors assuming that each blade is equipped with their own pitch motors. The drawback of IPC includes the increase in the usage of the pitch motors, which makes it vulnerable to wear.

The first part of this report introduces some of prospective smart blade technologies. The state-of-the-art review includes, along with smart structures and IPC, also LIDAR technology that can be used to estimate the incoming wind field. However, the main focus of the report is on the second part that deals with case study on pitch angle control. In the study, a basic simulation platform is set up, and several pitch angle controllers are tested. These controllers include a baseline Collective Pitch Controller (CPC) and IPC, as well as a Higher Harmonic Controller (HHC) that was adopted initially from helicopter applications. The controllers worked well, but also introduced several problems that are worth revisiting in the future.

Confidentiality	Public

Espoo 28.1.20111		
Written by	Reviewed by	Accepted by
Tuomas Haarnoja Research Scientist	Kari Tammi Research Professor	Pekka Koskinen Technology Manager

VTT's contact address
P.O. Box 1000, 02044 VTT

Distribution (customer and VTT)
VTT

Preface

The work described in this report has been carried out at VTT Industrial Systems in Smart Machines knowledge centre as a part of the VTT funded research project “Wind power plants - knowledge increase of noise and control issues” (WPPNoCo). The results were obtained through a literature survey and simulations in which the concepts of blade pitch angle control were verified and developed further. The work related to the controllers will be continued and the results will be submitted preliminarily to The 2011 International Conference on Power and Energy Engineering (CPEE2011) under the World Congress on Engineering and Technology 2011 (CET2011).

Espoo, 28.1.2011

Tuomas Haarnoja
tuomas.haarnoja@vtt.fi

Contents

Preface 2
1 Introduction 4
2 Emerging Technologies 5
2.1 Individual Pitch Control 5
2.2 Smart Structures 6
2.2.1 Background 6
2.2.2 Trailing-Edge Flaps 6
2.2.3 Microtabs 7
2.2.4 Camber Control 8
2.2.5 Active Twist 8
2.2.6 Boundary Layer Control 9
2.3 LIDAR 10
3 Case Study: Individual Pitch Control for Wind-Shear Compensation 11
3.1 Wind Turbine Reference Model 11
3.2 Controller overview 11
3.3 Collective Pitch Controller 12
3.3.1 Input Filter 12
3.3.2 Adaptive PI-Controller 13
3.3.3 Tuning 13
3.4 Baseline Individual Pitch Controller 16
3.5 Higher Harmonic Control (HHC) 18
3.6 Noise production 23
3.7 Future Work 24
4 Conclusions 25
5 Summary 25
Bibliography 26
Appendix A 27

1 Introduction

During the past decades, the size of wind turbines has been constantly been scaled up in order to minimize the overall cost of electricity. Currently, the manufacturers are working with up to 10 MW turbines; rotor diameters and hub heights exceeding over 100 meters. To make these extremely large turbines durable enough, their components are bulky, which in turn increases their weight and cost. Therefore, in a modern wind turbine the control system plays a significant role. By an intelligent control strategy, the fatigue loads can be minimized reducing the need for oversized components. Moreover, a modern controller can also be used to maximize the energy capture when the wind field is not ideal and to extend the wind speed range suitable for safe operation. On the other hand, the sophisticated controllers may need new kind of actuators that are able to produce the desired control outputs.

This report is organized as follows. Chapter 2 introduces some of the new technologies that have been studied to realize smart controllers. The chapter concentrates more on so called *smart structures* that can be used to modify the airfoil characteristic of individual blades. An older concept, Individual Pitch Control (IPC), is mentioned only shortly, as it will be studied more carefully in the case study in Chapter 3.

Before proceeding, it is important to understand that the control strategies discussed in this report are utilized in the third control region of a Variable-Pitch Variable-Speed (VPVS) controller. This is the region above a rated wind speed V_N at which the turbine is producing constant power and the rotor speed is fixed (Figure 1). At this region, the power capture of the rotor is worsen by adjusting the pitch angle out from the optimal orientation in order to keep the overall output power at the rated level. Although only the third operating region is considered in the case study, the same principles could be used in the other regions too.

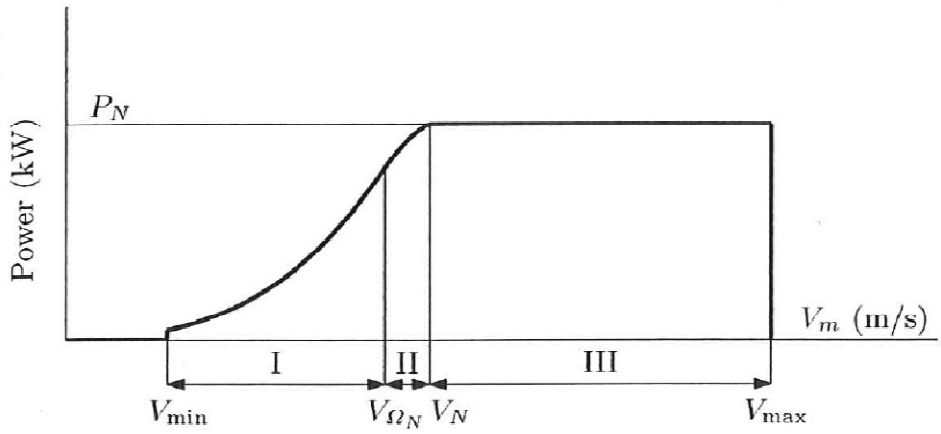

Figure 1 The three regions of operation. [1]

2 Emerging Technologies

2.1 Individual Pitch Control

Rapidly changing loads in large wind turbines can cause fatigue damage which reduces the life-span of the turbine and consequently increases cost of the electricity. The main contribution to the tilt and yaw moments that acts in the tower is wind shear: when a blade is in the upwards position, the axial force due to high wind is larger than the blade feels when pointing downward. This dissymmetry in the forces maps into an average tilt moment in the tower that tries to pull the hub downwind (Figure 2). In addition to the constant moment, there exists also periodic moments mainly at 1P (rotor angular frequency) and 2P (2*1P) and 3P (3*1P) frequencies. Also, similar force imbalance acts sideways resulting in a periodically varying yaw moment.

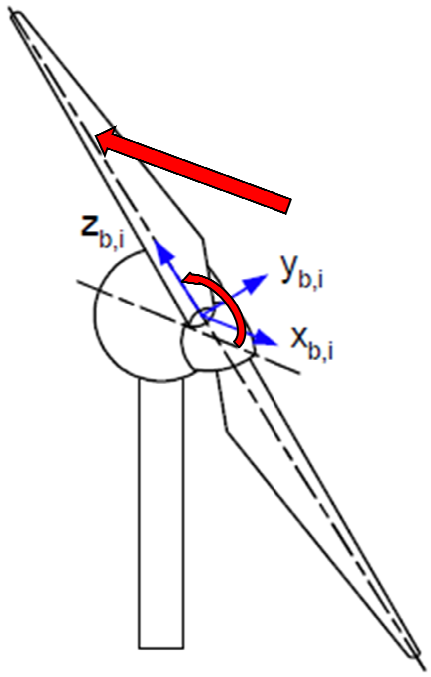

Figure 2 Resultant force acting above the hub and causing tilt and yaw moments. (Picture partly from [2])

In IPC, the pitch angles are controlled individually in a way that the aerodynamic force is kept constant during the revolution. This way the net axial force can be shifted to the center of the hub thus eliminating the tilt and yaw moments. The concept of individual pitch control is not new. The main problem associated with it is the excess use of the pitch motor that reduces its lifetime. Another problem is the large inertia of the blades that limits the achievable bandwidth. On the other hand, in modern wind turbines, each of the blade pitch angles are actuated with separate pitch motors, which makes the implementation of IPC quite simple. IPC is further considered in Chapter 3.

2.2 Smart Structures

2.2.1 Background

Smart structures in wind turbine blades mean sophisticated aerodynamic control surfaces that can be used for changing the local aerodynamic characteristics of the individual blades. The main benefits of such structures over ordinary IPC are in general their faster response time and lower rate of wear. Most commonly known of such structures are *flaps*, *microtabs*, *camber control*, *active twist,* and *boundary layer control*. These concepts as well as prospective actuators and sensors to realize smart structure control have been extensively studied in Delft University Wind Energy Research Institute (DUWIND) in the Netherlands and were reviewed *e.g.* by T.K. Barlas and G.A.M. van Kuik in [3]. This section cites their work and recaps the research of smart rotor control.

In order to apply active control, aerodynamic devices on the blades should be able to either change the characteristic $C_L - C_D - \alpha$ curve of the blade airfoil over specific sections or directly change the angle of attack (Figure 3). These coefficients describe how much lift and drag is achieved compared to the wind speed, and therefore they have also direct effect on the axial and radial force generated by the blades. The most important characteristics of these actuators include the change in the lift coefficient and the bandwidth they can provide [3]. The next subsections list several technologies that can be used to achieve desired change in either the airfoil or the incident angle.

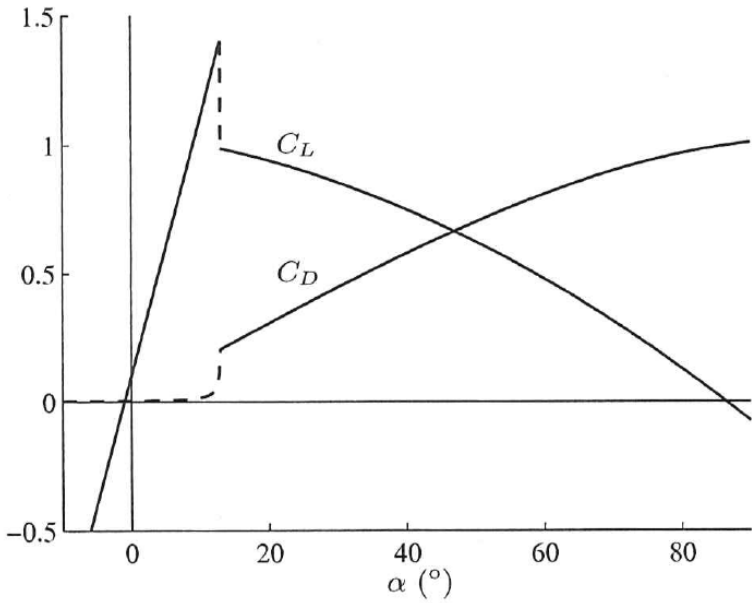

Figure 3 Lift (C_L) and drag (C_D) coefficients as a function of the angle of attach (α, the angle between wind and the chord of the blade). [1]

2.2.2 Trailing-Edge Flaps

Trailing-Edge Flaps are originally adopted from aircraft applications. The idea of the concept is to use small movable control surfaces, or *flaps*, to directly control lift on a blade airfoil. This technology seems promising for active load control because of its simplicity and effectiveness. By deploying the flaps on the pressure side the camber of the airfoil can be increases. Similarly, deployment on the suction side the camber can be decreased thus substantially changing the lift coefficient of the airfoil by altering the pressure distribution along the chord. Only small surface deflections are needed to achieve a significant change in the lift. Trailing-

edge flaps have also better structural and safety features than single shaft mechanisms and have substantially smaller power requirements than full or part span pitch control has. The low moment of inertia of the flaps also enables wide bandwidth control. Consequently such devices seem attractive to be used in the combination with smart materials for actuation. [3]

Trailing edge flaps can be employed in two manners: either as discrete flaps or as continuous deformable trailing edge (Figure 4). Discrete flaps (or *ailerons*) are hinged on the blade and require a moment over the hinge to achieve the required position. These kinds of flaps are generally promising but pose certain disadvantages. They do not comprise an integrated design solution, all the necessary mounting components are subject to wear and corrosion and the aerodynamic performance is reduced due to the sharp change in the camber. Furthermore, surface discontinuity triggers stall and poses noise issues. [3]

Continuous deformable trailing edge, or *variable trailing edge geometry,* results in a smooth change in shape, which makes it more effective and interesting integrated solution for an aerodynamic control device. This kind of device needs and actuator capable of producing smooth bending moment exerted over the flap. The actuators thus range from conventional motors to smart materials such as piezomaterials and shape memory alloys. This kind of structure have the drawback of making the actuator to work against the structural rigidity of the trailing edge and its skin will probably be subjected to fatigue. Actuating solutions range from conventional motors to smart material actuators such as piezoelectric materials or shape memory alloys. [3]

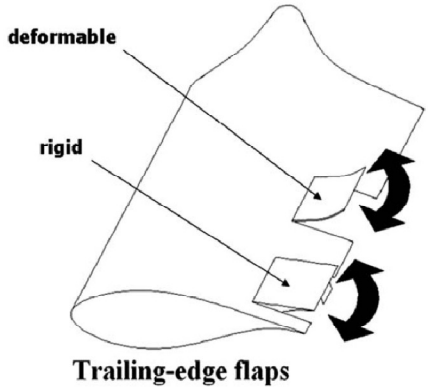

Figure 4 Two types of trailing edge flaps. [3]

2.2.3 Microtabs

Microtabs are small protruding devices placed near the trailing edge of an airfoil (Figure 5). The deployment of the tabs changes the trailing edge flow development and the effective camber of the airfoil providing thus changes in lift (Figure 6). The microtabs are deployed approximately normal to the surface and have a maximum length in the order of the boundary layer thickness, or 1–2 % of the chord. By deploying the tab on the pressure side of the airfoil, the lift coefficient can be increased. Similarly, deployment on the suction side results in reduction of lift. The tabs can also be placed near to the onset of pressure recovery in order to induce flow separation. Microtabs work mainly on on-off manner because their function is to change the effective camber of the airfoil by changing the trailing edge point. Nevertheless, variable change in lift can be achieved by spanwise deployment of microtabs. [3]

Microtabs have been shown to have an effect comparable to more conventional control surfaces such as trailing-edge flaps. One of the advantages of microtabs over flaps is their small-

er size that allows even faster response times. The tabs can be actuated by using *e.g.* piezoelectric materials. [3]

Figure 5 The concept of microtabs. [3]

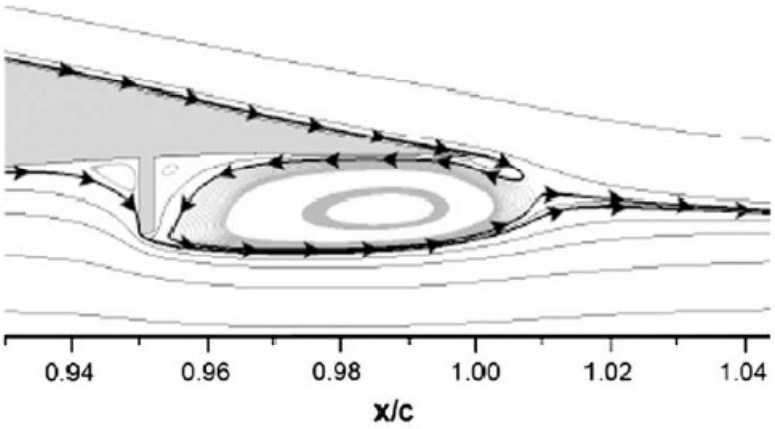

Figure 6 Microtab-induced flow in the airfoil trailing edge region. [3]

2.2.4 Camber Control

Camber control is another effective way of controlling the aerodynamic forces by directly changing the shape of the airfoil (Figure 7). This action has direct effects on the force distribution on the blade, so it can be used for active load alleviation purposes. This can be achieved generally by implementing smart materials inside the blade skin, or some kind of internal deformable structure. Such actuation process has to overcome all applied aerodynamic, dynamic and structural forces and deform the inner structure of the airfoil. Various concepts have been proposed for actuation, ranging from deformable construction for the center part of the chord to bending the aft section (or just the trailing edge). The former concept can be actuated by an internal framework which can be deformed by discrete actuators, or smart materials. [3]

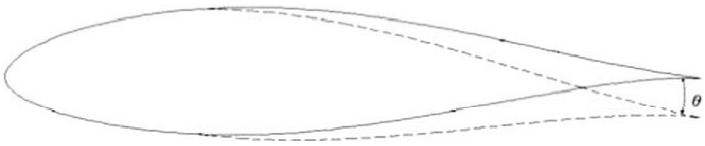

Figure 7 Concept of camber control. [3]

2.2.5 Active Twist

Trailing-edge flaps as well as microtabs were meant to change the airfoil characteristics directly. Active twist (Figure 8) is another type of concept, in which the aim is to change the lift and drag by adjusting the local angle of attack by actively changing the pitch angle of the whole blade or part of it as a function of distance from the hub. The largest change in the angle of attack is consequently in the blade tip that also has the largest contribution to the overall characteristics of the blade. With this concept, no spanwise distributed control of the blade is possible. Active twist has shown promising results in helicopter applications, but for a large scale wind turbine blades there evidently exists some disadvantages. First, the response time

for such a control concept will not be fast enough for active control purposes due to relatively large inertia. Also, the strains and control forces needed to twist the whole blade are estimated to be very high. [3]

For actuation purposes, smart materials are attached under the skin in fiber form or in the blade spar. In this way, small twist deflections can be achieved. This concept requires a torsional flexible design of the blade, which may make the blades prone to flutter. One of the biggest problems in the use of an active twist rotor is the large scale integration of smart materials in the torsion box or complete rotor blade structure. Especially the use of piezoelectric fiber composites would lead to a very heavy and expensive structure. A clear advantage of this concept is that a smooth rotor blade is obtained which does not change the aerodynamic behavior of the original blade design. [3]

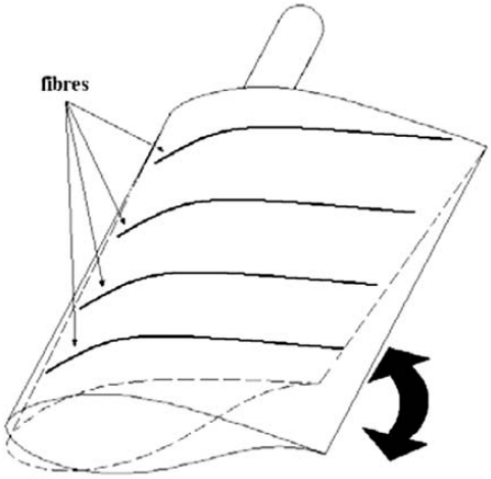

Figure 8 The concept of active twist. [3]

2.2.6 Boundary Layer Control

Yet another type of smart blade utilized boundary layer control. In this technique, the flow close to the surface of the airfoil is influenced to change the overall characteristics of the flow around the surface of the airfoil thus changing its effective airfoil characteristics. Most known of these methods are *boundary layer suction/blowing*, *synthetic jets*, *vortex generators* and *plasma actuators*, first two of which are presented below. These devices are located on the airfoil surface and used for separation control at moderate or large angles of attack. Besides boundary layer separation control, boundary layer control devices can also be used for camber control at lower angles of attack. [3]

The *boundary layer suction method* consists of a powered system to suck boundary layer flow from closely spaced vertical slots. The control of airfoils characteristics by suction is an old concept originating from first experiments in 1904. The technology evolved during the last century, and numerous experimental aircraft applications have been tested. The development of a boundary layer suction system is quite complicated, since it involves considerations on optimum slot placement, structural modifications, power system, amount of suction, *etc*. The main interest of this concept is the prevention of flow separation and the reduction of drag, but by using actively controlled suction, the virtual shape of the airfoil can be changed, so control in lift can be achieved in theory. [3]

Synthetic jets (Figure 9) are zero-net mass flux jets created by employing an oscillatory surface within a cavity. The jets are formed by alternating momentary ejection and suction of fluid across an orifice and are entirely created from the fluid that is being controlled, so no

fluid ducting is necessary. Net momentum addition and a change of direction are obtained because low momentum flow is removed from the boundary layer during the suction phase and high momentum flow is blown out perpendicular to the surface. The commonly used actuators are piezoelectric diaphragms, but other options of smart material actuators have also been considered. [3]

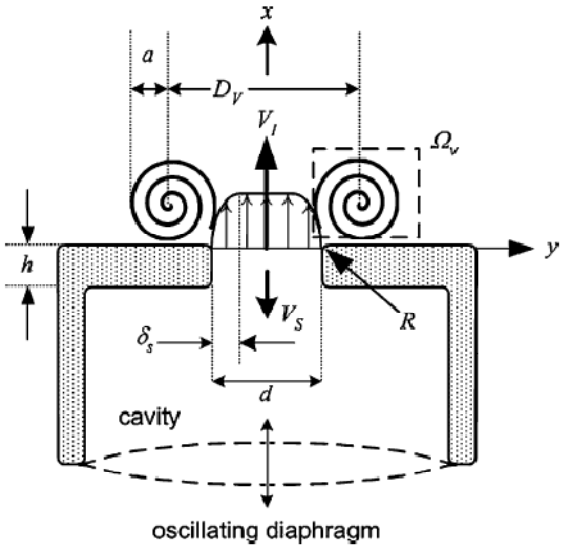

Figure 9 The structure of a synthetic jet. [4]

2.3 LIDAR

LIDAR (Light Detection and Ranging) has been recently introduced in wind turbine applications. The idea is to use a LIDAR to estimate the incoming wind field a few seconds beforehand. However, the research in this field is quite immature and demanding. The hardware costs are not at reasonable level, and the development of the wind field from the observation point to the rotor is challenging to model. Only after resolving these issues, a predictive controller can be developed. Due to these reasons, the LIDAR technique is not considered further in this report. Nevertheless, a possibly interesting field for future research could be the development of an optimal controller for a simulator, because that way the need for accurate wind modelling and expensive LIDAR system can be eliminated.

3 Case Study: Individual Pitch Control for Wind-Shear Compensation

The first objective of the case study was to implement a basic Collective Pitch Controller (CPC) for a reference 5-MW wind turbine model developed by National Renewable Energy Laboratory (NREL) [2]. The model was built by using NREL's wind turbine simulation software called Fatigue, Aerodynamics, Structures, and Turbulence (FAST) [5] [6]. The software is open source and written in Fortran. FAST models the wind turbine as a combination of rigid and flexible bodies. The aerodynamic torque from the rotor is modelled using AeroDyn subroutine package [7]. Although FAST includes a basic variable-speed variable-pitch controller, the user can implement his/her own controller as a Dynamic-Link Library (DLL). Alternatively, FAST can be compiled to generate a Matlab S-function. In this case study, the latter method is used.

The second objective was to improve the controller by adding an IPC to the model. Several different kind of IPCs were tested, ranging from the baseline IPC presented in [8] to more sophisticated Higher Harmonic Controllers (HHC) [9]. Appendix A summarizes the controller parameter values used in the simulations.

3.1 Wind Turbine Reference Model

The wind turbine model used in this case study is described in details in [2]. For convenience, the basic parameters are repeated in Table 1. The pitch actuator is not modelled in the setup, and therefore the actual pitch angle (θ) is exactly the same as desired pitch angle (θ_d) delayed by one integration time step. To make the model more realistic, the pitch angle was limited between 0 and +90 degrees and the angle rate between $\pm 8\ °/s$.

Table 1 Reference Wind Turbine Model Characteristics [2]

Rating	5 MW
Rotor Orientation, Configuration	Upwind, 3 Blades
Control	Variable Speed, Variable Pitch
Drivetrain	High speed, Multiple-Stage Gearbox
Rotor, Hub Diameter	126 m, 3 m
Hub Height	90 m
Cut-In, Rated, Cut-Out Wind Speed	3 m/s, 11.4 m/s, 25 m/s
Cur-In, Rated Rotor Speed	6.9 rpm, 12.1 rpm
Rated Tip Speed	80 m/s
Overhang, Shaft Tilt, Precone	5 m, 5°, 2.5°
Rotor Mass	110,000 kg
Nacelle Mass	240,000 kg
Tower Mass	347,460 kg
Coordinate Location of Overall CM	(-0.2 m, 0.0 m, 64 m)

3.2 Controller overview

The controller shown in Figure 10 was used in the third operating region (constant power + constant rotor speed). The controller consists of two separate sub-controllers, namely CPC

and IPC. CPC is used for keeping the wind turbine at the desired operating point (rated rotor speed + rated output power) by sending a common angle request for all of the three blade pitch motors. On the other hand, IPC is zero-average control signal that is tailored for each pitch motors separately. This additional pitch angle is used to alleviate some of the fatigue loads acting in the blades, drive train, and/or tower. The CPC and the IPC signals are then summed up and saturated to form the desired pitch angle request. The next section covers both the controllers in more detail. Throughout the study, the CPC block was kept the same, but the IPC was varied. The IPC shown in the figure is the baseline IPC against which the other IPCs are compared.

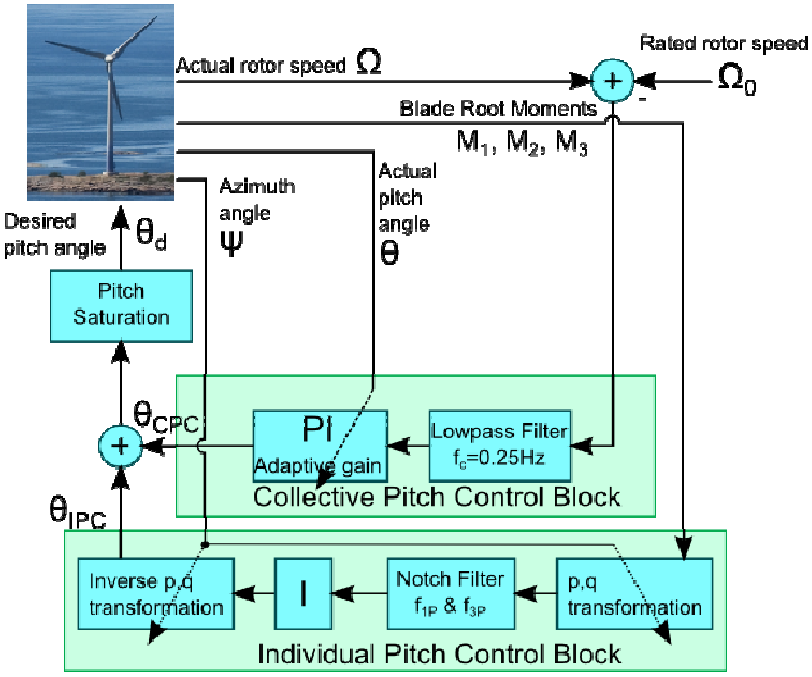

Figure 10 Block diagram for the individual pitch controller developed in the case study. p,q-transformation maps the blade loads from the rotating coordinate system to static coordinates in which a simple I-controller can be utilized to drive the average moments to zero.

3.3 Collective Pitch Controller

The CPC used in this example is also called as *baseline CPC* as it is commonly recognized as the most basic type of pitch controllers. The controller was developed according to the guidelines for the NREL's 5-MW reference wind turbine [2]. From Figure 10, two items can be identified in the CPC block: *input filter* and *adaptive PI controller*.

3.3.1 Input Filter

An exponential low-pass filter is used to filter out all the high-frequency components of the signal. The filter is a discrete-time exponential filter of type

$$y(n) = (1-\alpha)u(n) + \alpha y(n-1)$$
$$\alpha = \mathrm{e}^{-2\pi T_s f_c}$$

where $y(n)$ is the n^{th} measurement of the rotor speed, $u(n)$ is the corresponding output of the filter, T_s is the time step duration, and f_c is the cut-off frequency of the filter. The cut-off frequency that was used in this study was 0.25 Hz.

3.3.2 Adaptive PI-Controller

The collective pitch angle was controlled by using a PI controller. The D-term would only increase the effective moment of inertia of the system, and it was thus left out according to the recommendations in [10]. Because the dynamics from pitch angle to rotor angular speed is nonlinear, the PI controller cannot be used in its simplest form. The equation of motion for the rotor speed error $\Delta\Omega = \dot{\phi}$ for the closed-loop system is derived in [2]:

$$\underbrace{I_{\text{Drivetrain}}}_{M_\phi}\ddot{\phi} + \underbrace{\left(\frac{1}{\Omega_0}\left(-\frac{\partial P}{\partial\theta}\right)N_{\text{Gear}}K_{\text{P}} - \frac{P_0}{\Omega_0^2}\right)}_{C_\phi}\dot{\phi} + \underbrace{\left(\frac{1}{\Omega_0}\left(-\frac{\partial P}{\partial\theta}\right)N_{\text{Gear}}K_{\text{I}}\right)}_{K_\phi}\phi = 0, \tag{1}$$

where $I_{\text{Drivetrain}} = I_{\text{Rotor}} + N_{\text{Gear}}^2 I_{\text{Gen}}$ is the effective drive train moment of inertia of the Low-Speed Shaft (LSS), P is the rotor power (mechanical power) as a function of pitch angle (θ), N_{Gear} is the gear-box ratio, P_0 and Ω_0 are the rated mechanical power and rotor speed, and K_{P} and K_{I} are the PI controller tuning parameters. I_{Rotor} and I_{Gen} are the moments of inertia for the rotor (including the hub and LSS) and generator (including the High-Speed Shaft (HSS)). The characteristics of this second order system are defined by natural frequency

$$\omega_{\phi n} = \sqrt{\frac{K_\phi}{M_\phi}}$$

and damping ratio

$$\zeta_\phi = \frac{C_\phi}{2\sqrt{K_\phi M_\phi}} = \frac{C_\phi}{2M_\phi\omega_{\phi n}}.$$

The gains K_P and K_I can then defined by fixing the desired values of $\omega_{\phi n}$ and ζ_ϕ and solving the gains from (1) (and neglecting the small negative damping term $-\frac{P_0}{\Omega_0^2}$):

$$K_P = \frac{2I_{\text{Drivetrain}}\Omega_0\zeta_\phi\omega_{\phi n}}{N_{\text{Gear}}\left(-\frac{\partial P}{\partial\theta}\right)} \tag{2}$$

and

$$K_I = \frac{I_{\text{Drivetrain}}\Omega_0\omega_{\phi n}^2}{N_{\text{Gear}}\left(-\frac{\partial P}{\partial\theta}\right)}. \tag{3}$$

Hansen *et al.* [10] recommend using values of $\omega_{\phi n} = 0.6$ 1/s and $\zeta_\phi = 0.6$ to 0.7.

3.3.3 Tuning

The problem with the proposed PI-controller arises from the pitch sensitivity $\partial P/\partial\theta$ in (2) and (3) that is a nonlinear term in terms of pitch angle. A way to come over this issue is to use

PI controller gains that vary as a function of the pitch angle. Therefore, the sensitivity is needed to be measured from a linearized, uncontrolled system.

The sensitivity was measured using the linearization procedure documented in [2]. All unnecessary Degrees of Freedom (DoF) were disabled and a constant wind speed above the rated wind was applied to the rotor. A pitch angle was chosen so that it results in the rated power and rotation speed. The rotor power was set as plant output. The inbuilt linearization procedure was then used to gentle vary the pitch angle around this stable operating point, and the resulting variation in the rotor power was recorded. The same procedure was repeated for multiple wind speeds that all were above the rated wind speed. The results are presented graphically with the blue diamonds in Figure 11.

As seen from the figure, the sensitivity is quite linear function of the pitch angle. Therefore, the sensitivity term $\partial P/\partial\theta$ can be replaced by its linear approximation

$$\frac{\partial P}{\partial \theta} \approx \left(\frac{\partial P}{\partial \theta}\right)\Big|_{\theta=0} \left(1 + \frac{\theta}{\theta_K}\right),$$

where $(\partial P/\partial\theta)|_{\theta=0}$ is the sensitivity at zero pitch angle, and θ_K is the pitch angle at which the sensitivity has doubled.

Figure 11 also show the reference sensitivity results that were obtained by Jonkman *et al.* in [2] as red squares. The difference between these and our values is rather large, especially at small pitch angles. It also turns out, that the obtained controller is not stable unless the reference values were used. The difference between the two data sets is that the values got by Jonkman *et al.* are obtained by assuming a *frozen wake*. That means that the induced wake velocities are kept constant while perturbing the pitch angle in the linearization procedure. The reason behind this assumption is not fully studied in the scope of this report. Nevertheless when a modified copy of FAST (that makes the frozen wake assumption) is used, similar results were obtained (green triangles in Figure 11).

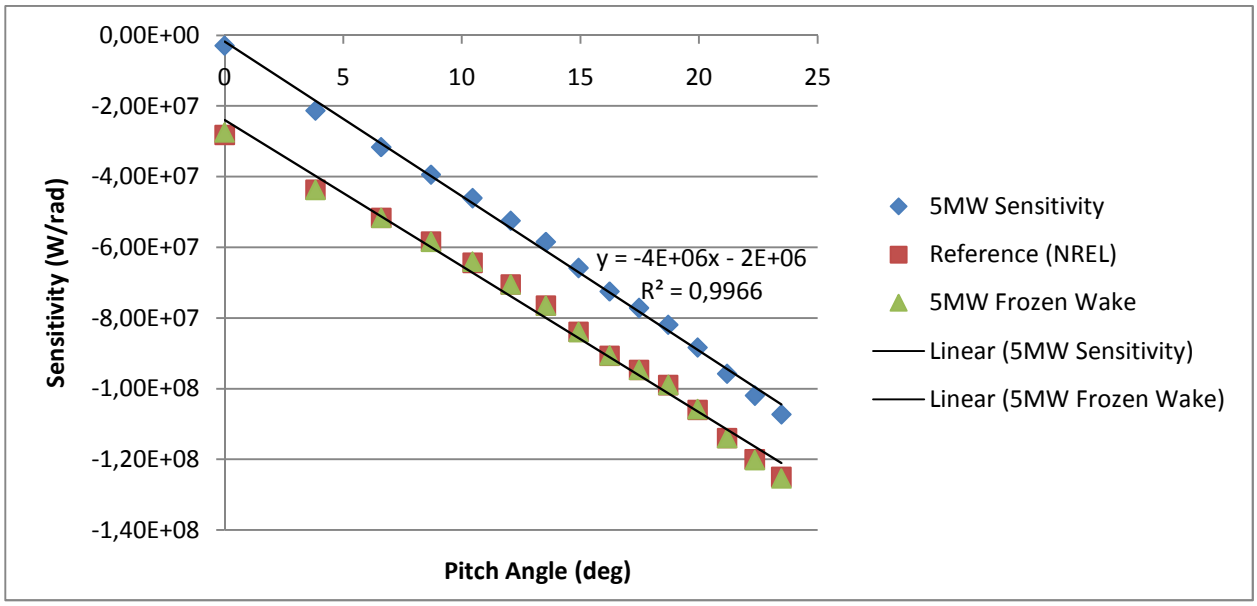

Figure 11 Sensitivity simulations for the NREL 5-MW reference wind turbine.

Next, a step response was simulated for the plain CPC. A homogenous wind field, which neglects also the wind shear, was used. After the system was settled down from the initial transients, a wind step of 1 m/s in magnitude was applied to the turbine. The step response was recorded in three different operating points: first at the minimum wind speed at which the turbine is operating in the region III, then at intermediate wind, and finally at maximum wind speed. The responses are shown in Figure 12. The actual input of the system, namely the wind speed, is not visible in the plots. Instead, the pitch angle is shown on the left and the output, *i.e.* rotor speed, on the right. Although the controller is tuned in order to have the same response characteristics regardless from the pitch angle, the system still reacts a bit differently at different operating points. At the slow wind speed (red curve), the system is under-damped, whereas at high speed (blue curve) it becomes over-damped. The intermediate wind speed (green curve) corresponds to the transition state in which the system is critically damped. One can also identify a vibration at about 0.4 Hz frequency. That vibration is the first harmonic of the fundamental rotor speed and excited presumably because of the precone angle that makes the incident angle of the blades to vary during a revolution.

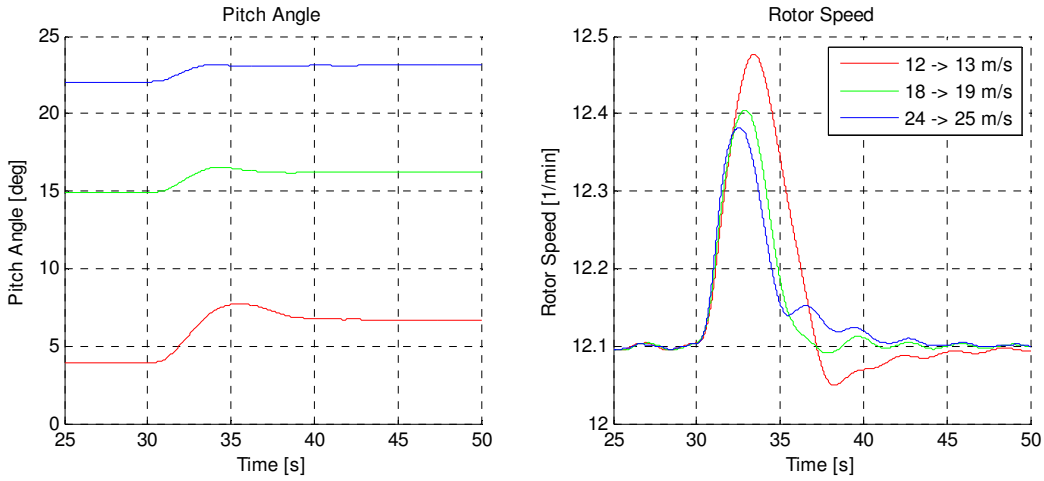

Figure 12 1 m/s wind speed step responses for the CPC controller at different wind speeds

Next, wind shear was added to the wind field and a simulation was run at fixed wind speed of 16 m/s. Wind shear is the main cause of fatigue stress that shortens lifetime of the wind turbine. This happens because the wind blow is stronger at the upper half of the rotor sweep area and weaker at the bottom. This wind gradient causes a constant moment that tries to tilt the whole tower. At low wind speeds, the static moment can also be dominated by the gravity, which causes a moment into opposite direction due to the precone angle. In addition, the rotating motion of the rotor causes a pulsating moment at $N_b\Omega$ frequency, where N_b is the number of blades, and Ω the angular speed of the rotor. Both the phenomena are visible in Figure 13 and Figure 14 in blue. Rotational sampling causes also similar varying moment around the yaw axis (marked as red). However, the reason for the static component in the yaw moment is not that obvious. Based on this simulation, it is obvious that the moments caused by wind shear are remarkable. The following simulations try to eliminate the static components of these two moments by utilizing an IPC.

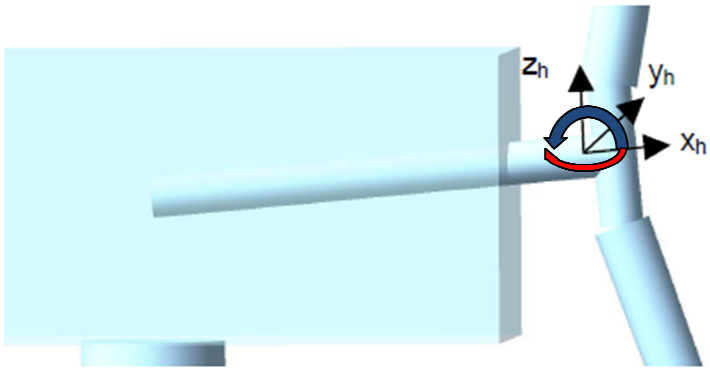

Figure 13 Resultant moments acting in the hub. Blue arrow corresponds to tilt moment and red arrow yaw moment. (Picture partly from [2])

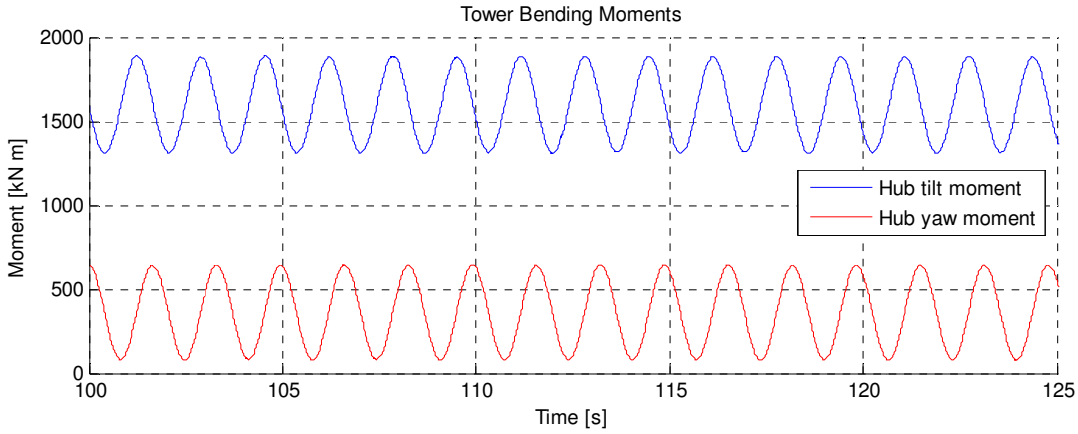

Figure 14 Disturbing moments acting in the hub due to wind shear at wind speed of 16m/s with wind shear.

3.4 Baseline Individual Pitch Controller

Next, a simple IPC was developed for the reference turbine. The controller used in this study is described by Wilson *et al.* in [11]. Wilson *et al.* combined the IPC with another controller utilizing smart structures to mitigate higher harmonic components of the disturbing loads. In this study, the IPC part was replicated and compared with their results.

The implementation of the IPC is based on the d-q transformation described in [8]:

$$\begin{bmatrix} M_d \\ M_q \end{bmatrix} = \frac{2}{3} \begin{bmatrix} \cos\phi & \cos\left(\phi + \frac{2\pi}{3}\right) & \cos\left(\phi + \frac{4\pi}{3}\right) \\ \sin\phi & \sin\left(\phi + \frac{2\pi}{3}\right) & \sin\left(\phi + \frac{4\pi}{3}\right) \end{bmatrix} \begin{bmatrix} M_1 \\ M_2 \\ M_3 \end{bmatrix},$$

where M_d and M_q are the yaw and tilt moment in the static rotor coordinate system; ϕ is the azimuth angle; and M_1 , M_2, and M_3 are the root bending moments of a three-blade rotor in the rotating rotor coordinate system. This way, the periodically varying blade root bending moments can be casted to a static coordinate system in which the plant can be treated as two

uncoupled SISO systems. These moments are then filtered to remove all disturbing resonance frequencies from the signal and then fed to an integrator. A plain I-controller is suitable to drive the average tilt and yaw moments to zero. Before feeding the control signals to the pitch motors, the signals have to be converted back to rotating coordinate system using an inverse d-q transformation defined by

$$\begin{bmatrix}\beta_1\\ \beta_2\\ \beta_3\end{bmatrix} = \begin{bmatrix} cos\phi & sin\phi \\ \cos\left(\phi+\frac{2\pi}{3}\right) & \sin\left(\phi+\frac{2\pi}{3}\right) \\ \cos\left(\phi+\frac{4\pi}{3}\right) & \sin\left(\phi+\frac{4\pi}{3}\right)\end{bmatrix}\begin{bmatrix}u_d\\ u_q\end{bmatrix},$$

where β_i is the pitch angle demand for i^{th} blade, and u_d and u_q are the integrator outputs for the yaw and tilt moments. Finally, the pitch angles are summed up with the collective pitch angle demand from the CPC and fed to the pitch motors.

The baseline IPC was used to compensate the dominating disturbances due to wind shear. Figure 15 shows the effect of the controller. Each of the blade pitch angles shown in the upper plot are periodically varied as a function of azimuth angle separated by 120 degrees in phase. The lower plot shows the resulting tilt and yaw moments as well as the blade root bending moment for blade 1, which is the moment that tries to bend the blade flap-wise in the rotating coordinate system (Figure 16). The amplitude of the 1P frequency of this moment is the main contributor for the static tilt and yaw moments in the hub. As seen in the plot, although the tilt and yaw moments are now zero on average, the IPC cannot completely eliminate the root bending moment because the controller sees only the net moment of all three blades. It is also worthy of remark that this disturbance is not purely sinusoidal, but it contains also higher harmonic frequency components. Consequently, although the controller is able to depress the static tilt and yaw moments to zero, a major factor causing fatigue of the blades remains also when utilizing the baseline IPC.

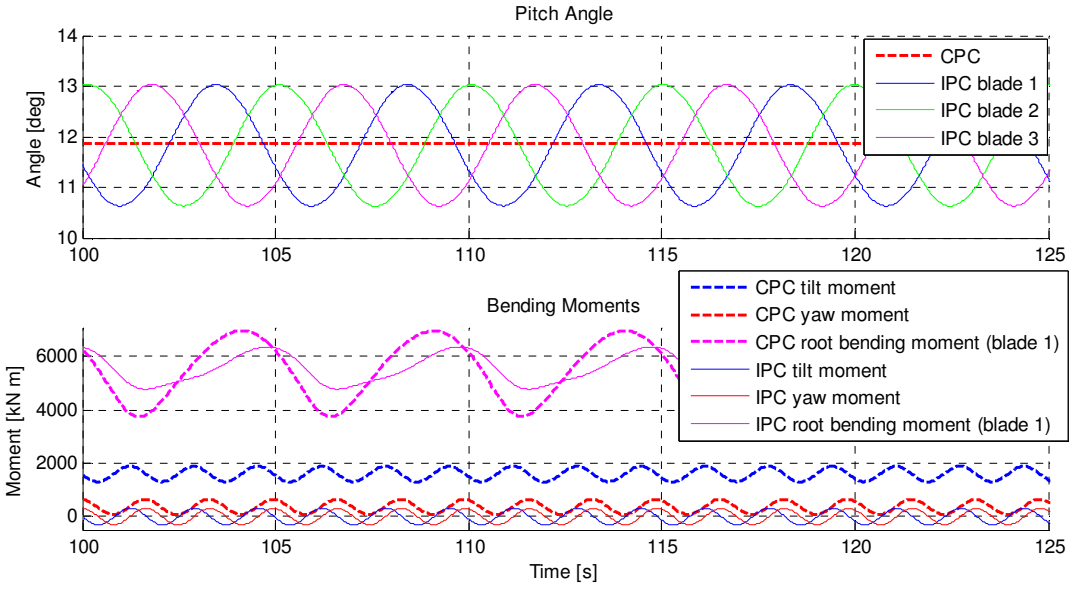

Figure 15 Comparison of CPC and IPC in terms of pitch angle and tilt and yaw moments.

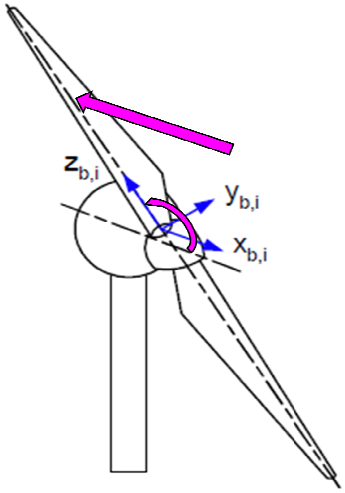

Figure 16 Root flap-wise bending moment. (Picture partly from[2])

3.5 Higher Harmonic Control (HHC)

In the previous baseline IPC, all the blade pitch angles are still coupled through the coordinate transformations. Another more sophisticated method for IPC was taken originally form helicopter applications [9]. This method is more general allowing actual independent control of the pitch angles and can be easily extended to include any disturbance frequency or its harmonic component. In this report, the method was taken to wind turbine application to eliminate the remaining disturbing moments in the tower and the blades.

The idea of HHC is to assume that the plant (in this case the wind turbine) can be treated as a quasisteady system. This means, that on the bandwidth of the controller the system can be considered to be in steady state. Using the assumption, the closed loop system at a specific frequency can be represented by

$$\boldsymbol{z} = \boldsymbol{T}\boldsymbol{u} + \boldsymbol{z_0},$$

where $\boldsymbol{z}$ contains the sine and cosine components (Fourier coefficient) of the blade vibration at the frequency of interest, $\boldsymbol{z_0}$ is the corresponding vibration amplitude for the nominal pitch angle (set by the CPC), $\boldsymbol{u}$ is the control signal amplitude, and $\boldsymbol{T}$ is a *constant control response matrix* containing the gain of the plant at the frequency of interest. The usage of $\boldsymbol{T}$ eliminates the need for knowing the overall transfer function of the plant.

Consequently, a simple feedback loop

$$\boldsymbol{u_{n+1}} = \boldsymbol{u_n} - \boldsymbol{T^{-1}}\boldsymbol{z_n}$$

should result in a deadbeat control. This control law for the N^{th} harmonic frequency is depicted in Figure 17 (Ω is the rotor angular speed). The output signal of the plant is first multiplied by cosine and sine signals that have the desired frequency. The product is then integrated over one or several periods of the disturbance frequency to get the Fourier components $\boldsymbol{z_n}$. The desired change in the input signal is then obtained by multiplying these coefficients by the inverse of constant control response matrix. A continuous time controller for the same system is derived in [9] and it is shown in Figure 18.

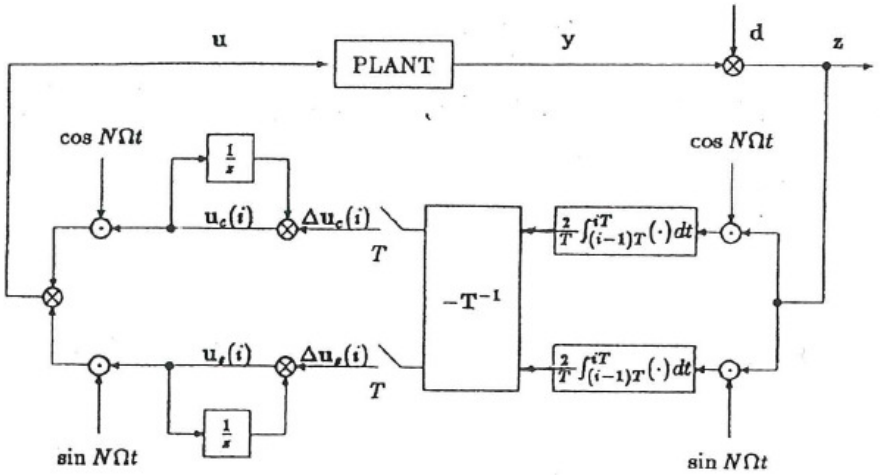

Figure 17 Discrete implementation for higher harmonic control system. [9]

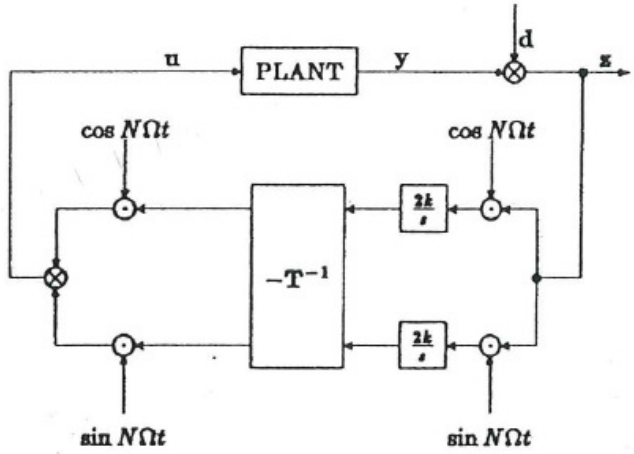

Figure 18 Continuous time controller for the system in Figure 17 [9].

The matrix $\boldsymbol{T}$ is identified from the plant $G(s)$ and it is given by

$$\boldsymbol{T} = \begin{bmatrix} T_{cc} & T_{cs} \\ T_{sc} & T_{ss} \end{bmatrix},$$

where

$$T_{cc} = T_{ss} = \text{Real}\{G(jN\Omega)\}$$
$$T_{cs} = -T_{sc} = \text{Imag}\{G(jN\Omega)\}.$$

In the wind turbine application, the output of the plant is the blade root bending moment and the input the desired pitch angle with respect to the operating point set by the CPC. Each of the blades needs to have their own controller. The HHC was implemented and tested using three setups: first setup was tuned only for 1P frequency; second for the frequencies 1P and 2P; and finally for 1P, 2P, and 3P. These controllers are referred to as HHC1, HHC12, and HHC123, respectively. A standard IEC turbulent wind of Type A and average speed 16 m/s was used, and the plant was simulated for 10 minutes. Figure 19 shows the Power Spectrum Density (PSD) for the root bending moments for the three HHCs as well as for the baseline

CPC and IPC for comparison. These results does not necessarily reflect to noise power associated to the disturbances, so any accurate conclusions about the quality of the controllers in the sense of reducing fatigue loads cannot be made. However, the graph gives an estimation of how well the controllers are able to alleviate the flapwise root bending moments as they were designed for. As seen in the graph, the baseline IPC reduces only the 1P component of the moment. The HHCs that are designed to work independently are, on the other hand, able to depress the 1P disturbance almost completely. Also HHC12 and HHC123 do the same for 2P, and HHC123 also for 3P frequencies.

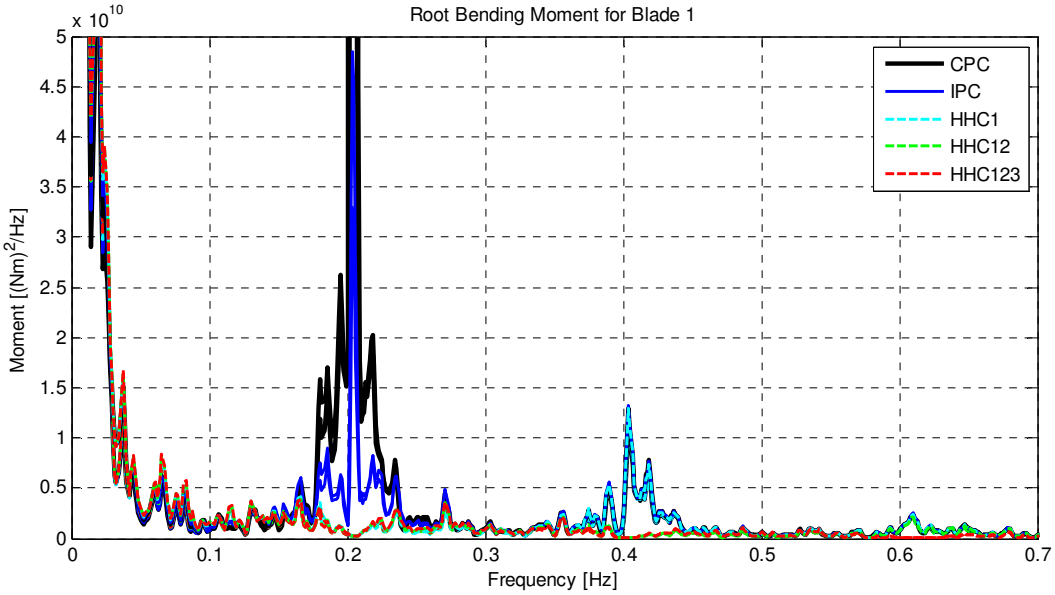

Figure 19 PSD of the root bending moment for various controllers. Wind used in the simulation was 16.0 m/s IEC Type A.

The results shown above were obtained by disabling the blade DOFs completely. This means that the blades were assumed to be rigid. This action was necessary because it turned out that the higher order HHC excited certain blade vibrations, which made it unable to depress the frequency components to which it is designed for. The effect of the blade DOFs is presented in Figure 20, which shows the PSD of the root bending moment for HHC123 both when the DOFs were enabled and disabled. For comparison, the figure also shows the baseline CPC with flexible blades (DOFs on). As seen in the figure, HHC123 makes the blades behave badly. The situation is the worse the more harmonic components are tried to be eliminated. Figure 21 illustrates the pitch angle of the same blade and simulations. From the figure, it is obvious that the vibrations are excited by the controller, either CPC or IPC. The reason for the poor performance of the controllers was not studied further in the scope of this project.

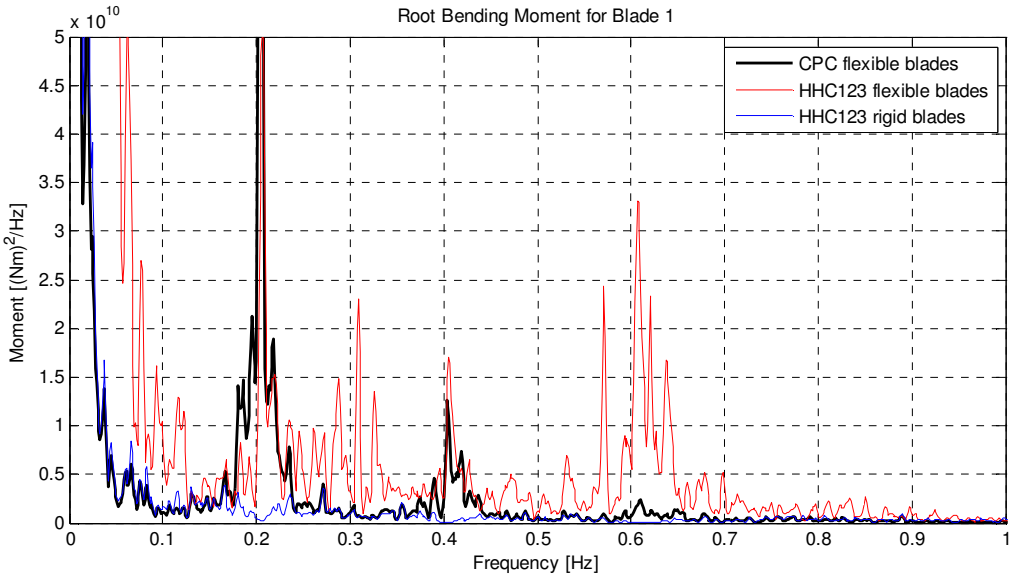

Figure 20 Comparison of root bending moment PSDs for rigid and flexible blades.

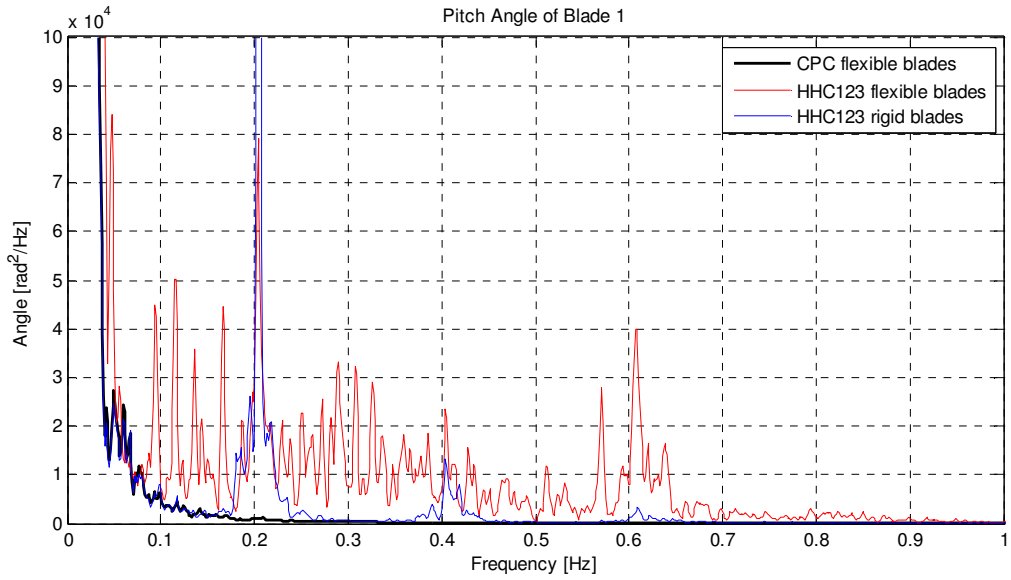

Figure 21 Comparison of pitch angle for rigid and flexible blades.

The IPC and the HHC increase obviously the usage of the pitch motor. Figure 22 shows an example of the pitch angle of blade 1 during the simulation. The variation around the collective angle (black curve) is about ± 2 degrees in this example. Since the dynamics of the pitch motor were not modelled, any exact estimation of the power usage of the motor cannot be made. However, a very simplified estimation can be made by assuming that the motor is working only against the moment of inertia of the blade neglecting forces caused by the rotational motion and interaction with the wind. In that case, the power needed is

$$P = \dot{\theta}T = \dot{\theta}\ddot{\theta}I_{rot}$$
$$\Rightarrow$$
$$P \propto \dot{\theta}\ddot{\theta},$$

where θ is the pitch angle, T is the torque of the pitch motor, and I_{rot} is the moment of inertia around the blade axis. Further, if the instantaneous power consumption is assumed to be always positive (no regenerative operation), a rough estimation for the average relative power consumption can be calculated (Table 2). These figures suggest that the usage of HHC for higher harmonic elimination should be carefully studied in order to justify its necessity.

Table 2 Relative Average Power Consumptions of the Controllers

Controller	Relative Power Consumption [-]
CPC	1.00
IPC	4.23
HHC1	11.37
HHC12	27.01
HHC123	48.14

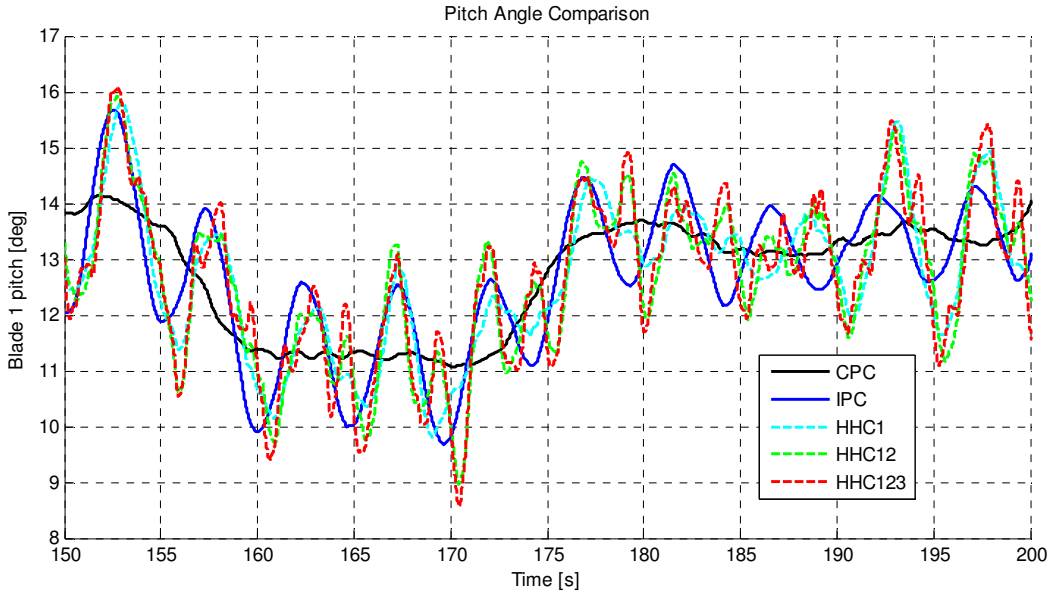

Figure 22 Comparison of pitch angle for blade 1.

Finally, the rotor torque for the controllers was compared to make sure the control strategies do not worsen the power output quality or expose the gear box to any additional torsional vibrations. Figure 23 shows the PSD for the rotor torques. HHC does not introduce any additional vibrations (as long as the blade DOFs are disabled). However, there exists some resonance peaks, most significant of which are at 0.6 Hz and 3.0 Hz. According to [2], the drivetrain natural frequency is at 0.62 Hz, which coincides with the first peak and its fifth harmonic with the one at 3.0 Hz. Because the torque affects directly the rotational speed of the rotor, similar peaks can also be identified in the angular speed and acceleration of the pitch angle control signal especially when utilizing higher harmonic controllers. It is also possible that the peaks are natural frequencies of the CPC or other controllers, such as the inbuilt torque or yaw controllers that were not covered here at all.

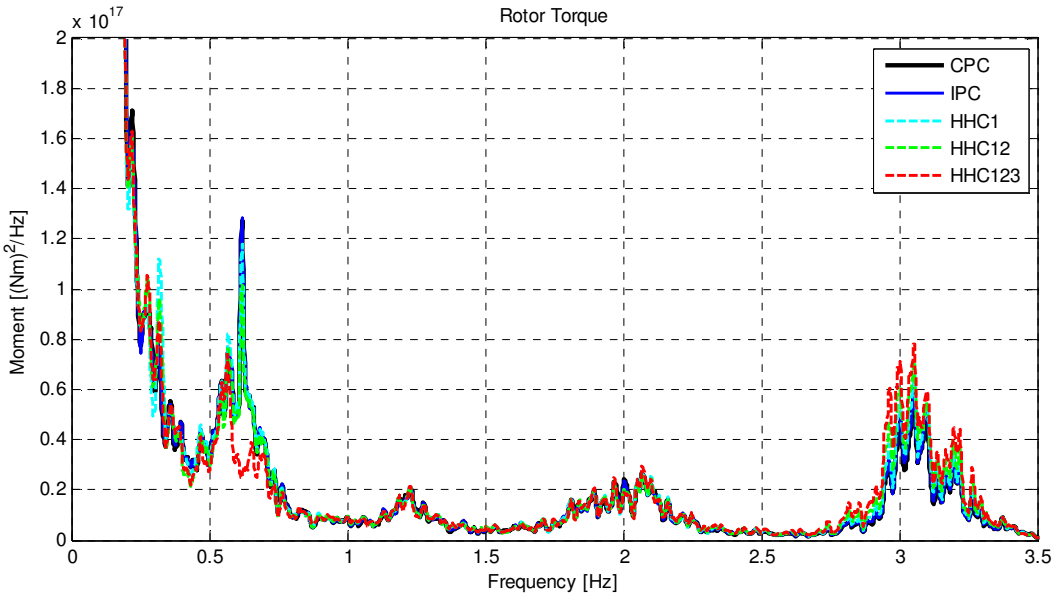

Figure 23 Comparison of rotor torque.

3.6 Noise production

There is also an inbuilt noise estimator in FAST. The noise prediction code is based on semi-empirical equations that predict six different noise sources that are assumed to be uncoupled from each other. These sources of noise are *turbulent boundary layer trailing edge*, *separating flow*, *laminar boundary layer vortex shedding*, *trailing edge bluntness vortex shedding*, t*ip vortex formation* and *turbulent inflow noise*. These models are covered in detail in [12]. The baseline CPC and IPC were compared in sense of their noise emission, and the noise pressure level was recorded at the distance of 100 meters in front of the turbine at the ground level. The spectra are shown in Figure 24. As can be seen in the chart, there is practically no difference in the noise level. However, no further conclusions should be made from the result, as neither the simulation method nor the noise calculations were verified in any sense. Especially, it should be noted that the noise prediction algorithm does not take into account the amplitude modulation of the noise, which has been shown the most disturbing characteristic of wind turbine noise.

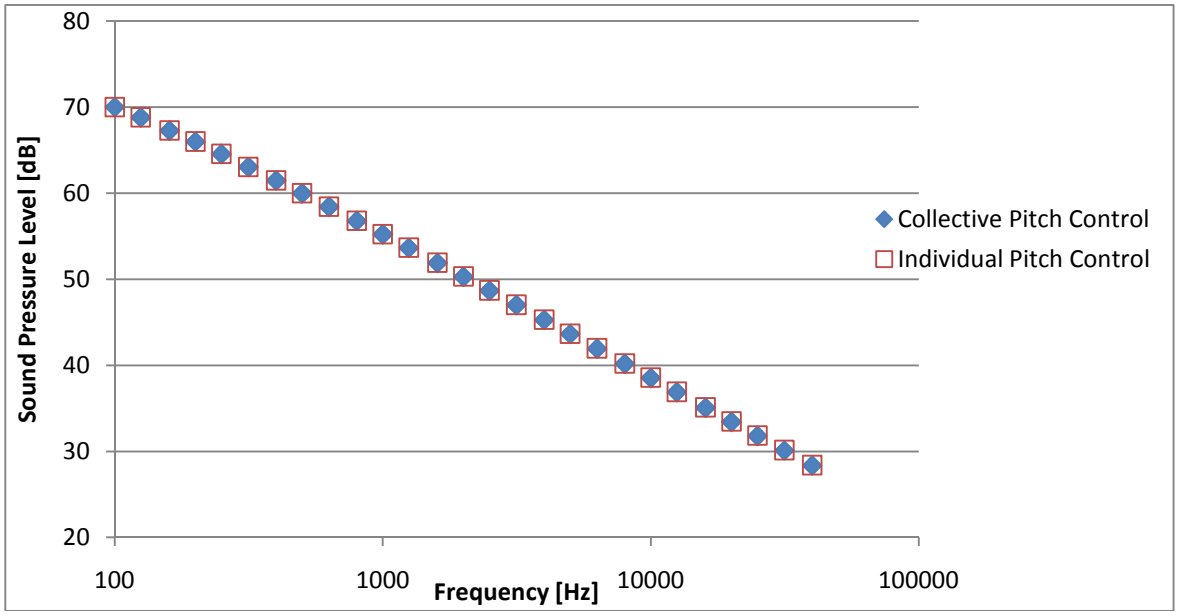

Figure 24 Noise spectra for the baseline CPC and IPC measured 100 upwind from the tower base.

3.7 Future Work

In the case study, several issues that are worth further research were identified. These ideas include the following points:

- How the DOFs in the blades affect the simulation. Why does not HHC work when the blade DOFs are turned on?
- Are there any real benefits of using the HHC instead of the baseline IPC? The former mitigates blade loads better but might excite other frequencies and requires more control effort.
- The usage of HHC requires information of the plant behaviour at the frequencies of interest (when determining $\boldsymbol{T}$). However, the behaviour is dependable on the pitch angle, possible wind speed, and azimuth angle, and consequently the identification process is not straightforward. How should the identification to be done and does it have any significant effect on the performance of the HHC?
- How to compare the quality of different controllers? A better estimation for the wear of the tower, blades, and drivetrain is needed to set the targets for the controllers. Also, a way to measure the pitch actuator wear is needed.
- What is the reason for the “frozen wake” assumption when tuning up the CPC? It is essential to understand the reason behind it when developing new CPC algorithms.
- What are the sources of the 0.6 Hz and 3.0 Hz vibrations in the drivetrain torque and consequently in the pitch angle control signal?

4 Conclusions

Smart blades and LIDAR technology were only introduced in this report and no further conclusions can be made regarding to their applicability to smart control of wind turbines. Nevertheless based on publication frequencies, these technologies are interesting, but not yet utilized in full scale commercial wind turbines. The wide bandwidth of the smart blades combined with predictive control based on the LIDAR technology could potentially provide an efficient way of reducing blade, drivetrain, and tower vibrations in the future.

A more mature control strategy is based on Individual Pitch Control. One of the biggest benefits of IPC is that it does not necessarily need any additional actuation in the rotor if the blades are already equipped with separate pitch motors. Although it has been shown by simulations and test facilities that IPC is an effective way of reducing loads in wind power plants, its migration to commercial products has been hindered by the drawback of wearing pitch motors. Consequently, IPC has to be always designed as a compromise between load reduction and the usage of the pitch motors. IPC may also have positive effect on the rotor power capture and noise production because it can be used to keep the angle of attach optimal during the revolution.

5 Summary

This report covered some technologies for smart control of wind turbines for load reduction. The smart blade structures were covered at the concept level, and more focus was paid on Individual Pitch Control. Several IPC approaches were tested in a case study, in which a blade pitch angle controller was developed for a NREL 5-MW wind turbine model. IPC was shown to be an effective way of reducing disturbances at 1P frequency but also excited blade vibrations when IPC was used to compensate the higher harmonic frequencies. IPC was also showed to increase the control effort significantly compared to the baseline Collective Pitch Controller.

Bibliography

1. **Bianchi, Fernando D., Battista, Hernán De and Mantz, Ricardo J.** *Wind Turbine Control System.* s.l. : Springer, 2007.

2. **Jonkman, J., et al.** *Definition of a 5-MW Reference Wind Turbine for Offshore System Development.* 2009. Technical Report.

3. *Review of state of the art in smart rotor control research for windf turbines.* **Barlas, T.K. and Kuik, G.A.M. van.** 2010, Progress in Aerospace Science, pp. 1-27.

4. *Formation Criterion for Synthetic Jets.* **Holman, Ryan, et al.** 2005, AIAA Journal, pp. 2110-2116.

5. **Jonkman, Jason.** FAST. [Online] 5 11 2010. [Cited: 7 12 2010.] http://wind.nrel.gov/designcodes/simulators/fast/.

6. **Jonkman, Jason M. and Buhl Jr., Marshall L.** *FAST User's Guide.* 2005. Manual.

7. **Laino, David J.** AeroDyn. [Online] 31 3 2010. [Cited: 7 12 2010.] http://wind.nrel.gov/designcodes/simulators/aerodyn/.

8. *Individual Blade Pitch Control for Load Reduction.* **Bossanyi, E. A.** 2, 2003, Wind Energy, Vol. 6, pp. 119-128.

9. *Linear Control Issues in the Higher Harmonic Control of Helicopter Vibrations.* **Hall, Steven R. and Wereley, Norman M.** Boston, MA : s.n., 1989. 45th Annual forum of the American Helicopter Society. pp. 955-971.

10. **Hansen, Morthen H., et al.** *Control design for a pitch-regulated, variable speed wind turbine.* Roskilde : s.n., 2005. Technical Report.

11. *Combined Individual Pitch Control and Active Aerodynamic Load Controller Investigation for the 5MW UpWind Turbine.* **Wilson, David G., et al.** Chicago, Illinois : s.n., 2009. AWEA Windpower 2009.

12. **Moriarty, P. and Migliore, P.** *Semi-Empirical Aeroacoustic Noise Prediction Code for Wind Turbines.* Golden, Colorado : National Renewable Energy Laboratory, 2003. Technical Report.

Appendix A

Symbol	Value	Explanation
$\boldsymbol{f_c}$	0.25 Hz	Cut-off frequency of the CPC input filter
$\boldsymbol{T_s}$	0.0125 s	Integration time step
$(\partial P/\partial\theta)\vert_{\theta=0}$	-25.52e6 W/rad	Rotor power sensitivity at zero pitch angle
θ_k	6.302336°	Pitch angle at which the rotor power sensitivity has doubled
$K_{I,IPC}$	1e-6	IPC integrator gain
$\boldsymbol{T}^{-1}$	$\begin{bmatrix} -2.1571\text{e}-5 & 0 \\ 0 & -2.1571\text{e}-5 \end{bmatrix}$	Inverse of constant response matrix for all frequencies
ζ_ϕ	0.7	CPC damping coefficient
$\omega_{\phi n}$	0.6	CPC natural frequency
Ω_0	12.1 rpm	Rated rotor speed